Acta Pharmaceutica Sinica B 2022;12(4):2000–2013

Chinese Pharmaceutical Association
Institute of Materia Medica, Chinese Academy of Medical Sciences

Acta Pharmaceutica Sinica B

www.elsevier.com/locate/apsb
www.sciencedirect.com

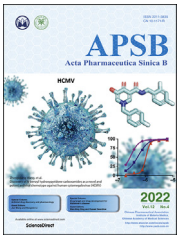

ORIGINAL ARTICLE

Engineered platelets-based drug delivery platform for targeted thrombolysis

Songli Wang[a,c], Ruifeng Wang[a], Nana Meng[a], Linwei Lu[b], Jun Wang[a], Jianfen Zhou[a], Jiasheng Lu[a], Qianzhu Xu[a], Cao Xie[a], Changyou Zhan[a,c], Yao Li[d], Yang Yu[d], Weiyue Lu[a,e,f,*], Min Liu[a,*]

[a]*Department of Pharmaceutics, School of Pharmacy, Key Laboratory of Smart Drug Delivery (Ministry of Education and PLA), Fudan University, Shanghai 201203, China*
[b]*The Department of Integrative Medicine, Huashan Hospital, Fudan University and the Institutes of Integrative Medicine of Fudan University, Shanghai 200041, China*
[c]*Department of Pharmacology, School of Basic Medical Sciences, Fudan University, Shanghai 200032, China*
[d]*The National Facility for Protein Science in Shanghai (NFPS), Shanghai 201210, China*
[e]*State Key Laboratory of Medical Neurobiology and the Collaborative Innovation Center for Brain Science and Department of Pharmacology, School of Basic Medical Sciences, Fudan University, Shanghai 200032, China*
[f]*Minhang Branch, Zhongshan Hospital and Institute of Fudan-Minhang Academic Health System, Minhang Hospital, Fudan University, Shanghai 201199, China*

Received 15 October 2021; received in revised form 29 December 2021; accepted 31 December 2021

KEY WORDS

Platelet;
Urokinase;
Nitric oxide;
Targeted thrombolysis;
Thrombus reformation

Abstract Thrombolytic agents have thus far yielded limited therapeutic benefits in the treatment of thrombotic disease due to their short half-life, low targeting ability, and association with serious adverse reactions, such as bleeding complications. Inspired by the natural roles of platelets during thrombus formation, we fabricated a platelet-based delivery system (NO@uPA/PLTs) comprising urokinase (uPA) and arginine (Arg) for targeted thrombolysis and inhibition of re-embolism. The anchoring of uPA to the platelet surface by lipid insertion increased the thrombotic targeting and *in vivo* circulation duration of uPA without disturbing platelet functions. Nitric oxide (NO) generated by the loaded Arg inhibited platelet aggregation and activation at the damaged blood vessel, thereby inhibiting re-embolism. NO@uPA/PLTs effectively accumulated at the thrombi in pulmonary embolism and carotid artery thrombosis model mice and exerted superior thrombolytic efficacy. In addition, the platelet delivery system showed excellent thrombus recurrence prevention ability in a mouse model of secondary carotid artery injury. The coagulation indicators *in vivo* showed that the platelet-based uPA and NO co-delivery system possessed a low hemorrhagic risk, providing a promising tool for rapid thrombolysis and efficient inhibition of posttreatment re-embolism.

*Corresponding authors. Tel./fax: +86 21 51980090 (Weiyue Lu); +86 21 51980092 (Min Liu).
E-mail addresses: wylu@shmu.edu.cn (Weiyue Lu), liumin@shmu.edu.cn (Min Liu).

Peer review under responsibility of Chinese Pharmaceutical Association and Institute of Materia Medica, Chinese Academy of Medical Sciences.

https://doi.org/10.1016/j.apsb.2022.01.004

1. Introduction

Thrombotic vascular diseases partially or completely block the blood flow in the blood vessels, block the supply of oxygen and nutrients to the cells, cause ischemia and necrosis of the corresponding downstream tissues, and then lead to life-threatening diseases such as acute myocardial infarction, ischemic stroke, and pulmonary embolism[1−4]. The main treatment for thrombotic vascular disease is timely and rapid thrombolysis to restore blood flow supply and prevent thrombus regeneration. Thrombolytic drugs such as tissue plasminogen activator (tPA) infusion by systemic administration or catheter infusion have greatly improved the survival rate and quality of life of patients[1,2]. However, current treatment methods have some drawbacks. For example, the short half-life of thrombolytic drugs (usually only a few minutes) and the lack of targeting (less than 5% of the drug reaches lesion site) require multiple high-dose systemic administrations, which not only increases healthcare costs but also causes side effects such as thrombolytic resistance, bleeding, and unstable blood pressure[5−7]. At the same time, simple thrombolytic strategies are unable to meet clinical needs due to the complexity of the causes of thrombosis. Drug injections alone also carry the risk of recurrence of thrombosis due to a failure to eliminate inflammation at the thrombus site, with only 2%−7% of patients benefiting from thrombolytic therapy[8−10]. To improve patient prognosis, there is an urgent need to develop a thrombus-targeted thrombolytic drug delivery strategy that enhances the thrombolytic effect while eliminating thrombus site inflammation to prevent thrombus regrowth, ensure blood flow re-establishment and reduce systemic side effects.

Targeted delivery of thrombolytic drugs that directly improve thrombolysis has shown promise in preclinical studies[11−15]. Rotating magnetic nanomotors enhanced the transport of tPA at the blood–clot interface, thereby accelerating the rate of thrombolysis and improving thrombolytic efficacy[16]. To improve targeting efficiency, synthetic materials bound to targeting ligands have been applied[17,18]. Inspired by the pathophysiological functions played by platelets during thrombosis, Pawlowski et al.[19] utilized a liposome platform with a surface modified by platelet targeting ligands. Based on the properties of annexin-V binding to phosphatidylserine, Pan et al.[20] designed annexin-V conjugated micelles for targeted delivery of lumbrokinase (LBK) to lyse thrombi. However, the immunogenicity of the polypeptide molecules conjugated to the preparation surface and the formation of a protein corona on the preparation surface attenuate the thrombus targeting ability and limit the clinical transformation of the artificially designed drug delivery system.

In addition to directly improving thrombolysis, the inhibition of thrombosis recurrence is another critical point for thrombus rescue. In thrombotic diseases, especially arterial thrombosis, platelets first adhere to damaged vascular endothelial cells and then become activated and aggregate to form initial platelet emboli[21]. NO, as a potent inhibitor of platelet activation and aggregation, can block thrombus formation at the initial stage of thrombosis and prevent thrombus regeneration[22−24]. Preclinical studies have been conducted with the aim of preventing thrombosis by coating NO on stents or other medical devices that are in contact with the vessel wall[25,26]. Endogenous NO is synthesized and released in endothelial cells or platelets by NO synthase (NOS)[27,28]. Delivery of NO donors, such as Arg, isosorbide dinitrate, and nitroglycerin, provides an alternative NO delivery strategy for inhibition of thrombosis recurrence.

Platelets maintain vascular integrity under physiological conditions and are involved in thrombus formation under pathological conditions. Based on their functions in thrombus targeting and immune escape, platelets and platelet-like bionanoparticles show promise in stroke diagnosis, atherosclerosis treatment and targeted thrombolysis[29−31]. We speculate that a platelet-based drug delivery system may be able to effectively target the platelet-rich thrombus site, enhance the thrombolytic effect and release NO to prevent thrombus recurrence.

In this work, inspired by the glycosylphosphatidylinositol anchoring protein on the plasma membrane, thrombolytic drugs were anchored onto the platelet surface by platelet surface anchoring engineering techniques[32−34]. As shown in Fig. 1, phospholipid-linked uPA was first synthesized and then anchored to the platelet membrane surface by lipid insertion without affecting platelet function. Intracellularly encapsulating Arg conferred a therapeutic effect on this platelet delivery system for rapid targeted thrombolysis and prevention of thrombus recurrence. Thrombolysis experiments in mouse pulmonary and carotid artery thrombosis demonstrated the powerful natural targeting and enhanced thrombolytic effect of uPA-anchored platelets. A mouse carotid artery secondary injury assay demonstrated the excellent thrombus recurrence prevention ability of NO@uPA/PLTs. Compared to free uPA, platelet preparations (uPA/PLTs, NO@uPA/PLTs) with chimaeric uPA had a lower effect on the mouse coagulation system and exhibited a lower risk of bleeding. The uPA- and Arg-coloaded platelet delivery system provides a safe and practical strategy for the treatment of thrombosis-related diseases and prevention of thrombotic recurrence.

2. Materials and methods

2.1. Materials

uPA and L-Arg were purchased from Aladdin Chemistry Co., Ltd. (Shanghai, China). Cy5-NHS (*N*-hydroxysuccinimide), DAF-FM diacetate (4-amino-5-methylamino-2,7-difluorofluorescein diacetate), FDA (fluorescein diacetate), DiD (1,1′-WGA-Alexa 488ctadecyl-3,3,3′,3′-tetramethylindodicarbocyanine, 4-chloro benzenesulfonate salt dye), WGA-Alexa 488 (3,3′-WGA-Alexa 488ctadecyloxacarbocyanine perchlorate), thrombin, ADP (adenosine diphosphate), fibrinogen, rhodamine 6G, ferric chloride ($FeCl_3$) and phosphate-buffered saline (PBS) were purchased from Meilun Biology Technology Co., Ltd. (Dalian, China). NHS-

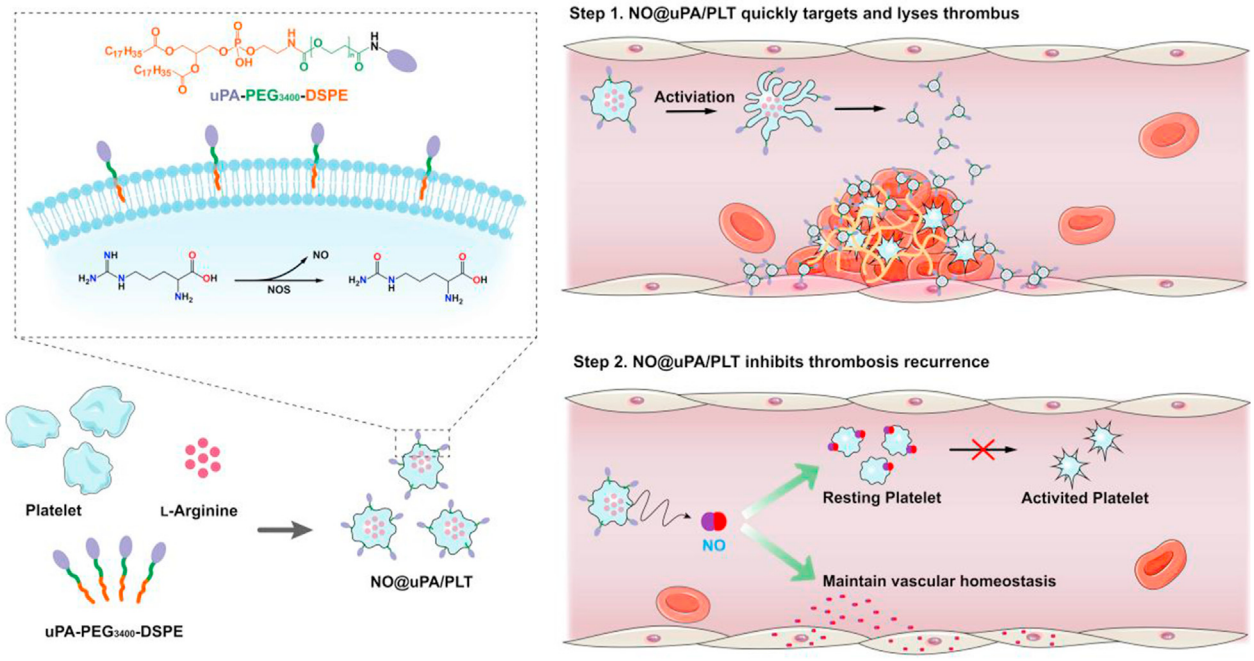

Figure 1 Illustration of the engineered platelet-based drug delivery platform. The uPA/Arg coloaded platelet delivery system provided a unique combination to achieve targeted delivery of uPA to thrombi, prolong the circulation duration of uPA and prevent the recurrence of thrombi with limited haemorrhagic risk.

PEG_{3400}-DSPE was purchased from Shanghai ToYongBio Tech. Inc. (Shanghai, China). Bovine serum albumin (BSA), glucose, dimethyl sulfoxide (DMSO), dichloromethane (DCM) was from Sinopharm Chemical Reagent Co., Ltd. (Shanghai, China). Other chemicals used in this project are analytical reagents. ICR mice (male, 20−25 g body weight) were purchased from the Sippr-BK Laboratory Animal Co., Ltd. (Shanghai, China) and kept under SPF conditions. All animal experiments were conducted in accordance with guidelines evaluated and approved by the Ethics Committee of Fudan University.

2.2. *Fluorescent labeling*

Proteins (uPA, fibrinogen) dissolved in sodium bicarbonate buffer (0.1 mol/L, pH 8.3) were reacted with a 2-fold excess of Cy5-NHS. After 2 h incubation at room temperature, excess Cy5-NHS was removed by Zebra column. The fluorescent-labeled proteins were obtained.

2.3. *Synthesis of uPA-PEG_{3400}-DSPE*

uPA (1 mg/mL, in PBS) was reacted with a 1.2-fold excess of NHS-PEG_{3400}-DSPE (10 mg/mL, in DMSO). After 4 h incubation at room temperature, excess NHS-PEG_{3400}-DSPE was removed by Zebra column. The synthesis of uPA-PEG_{3400}-DSPE was confirmed by SDS-PAGE analysis on a Bio-Rad Mini-PROTEAN TGX Stain-Free 4%−20% acrylamide gel.

2.4. *Preparation of platelets*

Murine whole blood was isolated from orbital vein and anti-coagulated with trisodium citrate. Platelet-rich plasma (PRP) was separated after centrifugation (200 $\times g$, 12 min) at room temperature. And prostaglandin E1 (Sigma−Aldrich) was added to PRP with a final concentration of 1 μmol/L. Then the PRP was centrifuged at room temperature (500 $\times g$, 12 min) to pellet the platelets.

2.5. *Preparation and characterization of NO@uPA/PLTs*

The platelet pellet was mixed with various concentrations of uPA-PEG_{3400}-DSPE and Arg in PBS. Then the mixture was stirred with low speed at 37 °C for 30 min, and platelets were washed 3 times in calcium-free Tyrode's buffer. The Western blotting analysis was performed to verify the loading of uPA. The loading amount of uPA was determined by the chromogenic substrate method. The loading amount of Arg was determined by detection of Arg concentration before and after incubation with platelets. The size of resting and activated NO@uPA/PLTs was measured using Zetasizer (Malvern). The morphology of resting and activated NO@uPA/PLTs was visualized using TEM and SEM. The fluorescent resting and activated NO@uPA/PLTs was imaged by the laser scanning confocal microscope (Leica SP8, Germany).

2.6. *Pharmacokinetics of NO@uPA/PLTs*

The mice were intravenously injected with Cy5-PLTs, Cy5-uPA/PLTs, and Cy5-NO@uPA/PLTs. At specified time points, the blood was collected and centrifuged to obtain platelets (including Cy5-uPA/PLTs or Cy5-NO@uPA/PLTs). The percentage and fluorescent intensity of Cy5-uPA/PLTs or Cy5-NO@uPA/PLTs was measured by Flowjo software.

2.7. *In vitro study of fibrin-binding ability*

NO@uPA/PLTs were dispersed in calcium-free Tyrode's buffer (134 mmol/L NaCl, 3 mmol/L KCl, 0.3 mmol/L NaH_2PO_4,

2 mmol/L $MgCl_2$, 5 mmol/L HEPES, 5 mmol/L glucose, 0.1% $NaHCO_3$, and 1 mmol/L EGTA, pH 7.4), and adjusted to a platelet concentration of 2×10^8/mL for activated NO@uPA/PLTs, 1 U/mL of thrombin was dissolved in the calcium-free Tyrode's buffer. To assess the fibrin-binding ability of NO@uPA/PLTs, NO@uPA/PLTs dispersed in calcium-free Tyrode's buffer with or without thrombin were incubated with Cy5-labeled fibrinogen for 30 min. Then NO@uPA/PLTs were collected by centrifugation at 500 $\times g$ for 8 min. All samples were washed three times in calcium-free Tyrode's buffer and analyzed by flow cytometry.

2.8. *In vitro study of activated endothelial cell binding ability*

Human umbilical endothelial vascular cells (HUVEC) were cultured in Dulbecco's modified Eagle's medium (Gibco) supplemented with 10% FBS (Gemini) at 37 °C under a humidified atmosphere containing 5% CO_2. Activated HUVEC were obtained by stimulating with TNF-α (50 ng/mL) for 24 h. For flow cytometric analysis, both activated and inactivated cells were fixed with 4% phosphate-buffered paraformaldehyde for 30 min at 4 °C and blocked with 20% mouse serum for 30 min. Then the cells were dyed with WGA-Alexa 488 and incubated with Cy5-NO@uPA/PLTs. After incubated for 30 min at 4 °C, the cells were washed three times with cold PBS to remove unbound NO@uPA/PLTs. Data were collected using a FACSCanto II flow cytometer (BD Biosciences) and analyzed by Flowjo software. For confocal microscopy imaging, cells stained by DAPI and WGA-Alexa 488 sequentially were subjected to the same processing steps as flow cytometry experiments. Confocal microscopy was conducted using a Leica SP8. The expression of ICAM-1, VCAM-1, and E-selectin in HUVEC before and after activation by TNF-α was also evaluated by flow cytometry. The same steps as described above flow cytometric analysis were followed. Then the cells were incubated with anti-ICAM-1 antibody, anti-VCAM-1 antibody, and anti-E-selectin antibody dissolved in 3% BSA solution for 30 min at 4 °C, respectively. The cells were then washed three times with cold PBS and the collected cells were detected by flow cytometry and the data were analyzed using Flowjo software.

2.9. *Thrombolysis evaluation in vitro*

Dynamic thrombolysis assessment by microfluidic studies. uPA, uPA/PLTs, and NO@uPA/PLTs were flowed through a parallel plate flow chamber (Glycotech, USA) coated with fluorescence-labeled fibrin clot for 35 min at 20 dyne/cm^2. Fluorescence-labeled fibrin clot was prepared by mixing Cy5 labeled fibrinogen solution (5 mg/mL, 150 μL), thrombin solution (3 U/mL, 30 μL), calcium chloride solution (0.5 mol/L, 10 μL), ADP solution (5 μmol/L, 10 μL), spreading on the acid-washed and dried slides and incubating at 37 °C for 30 min. Images were obtained with an Observer Z.1 Inverted Microscope (Zeiss, Germany). The fluorescent intensity of fluorescence-labeled fibrin clot was quantified using ImageJ software.

2.10. *In vivo clot-targeting studies*

A mouse pulmonary embolism model was made by injecting thrombin intravenously. Then Cy5 labeled uPA/PLTs and NO@uPA/PLTs were injected intravenously respectively. The mice were euthanized 30 min after the injection of thrombin, and then lung tissues of the mice were obtained. IVIS was used to image mouse lung tissue and Living Image software was used to semi-quantitate the fluorescence intensity of Cy5 through region-of-interest (ROI) analysis. To observe the intrapulmonary distribution of NO@uPA/PLTs, FITC-fibrinogen and NO@Cy5-uPA/PLTs were used instead. The obtained mouse lung tissues were treated by freezing microtomy. The frozen sections of lung tissue were stained with DAPI and then observed using a confocal microscope (Leica SP8).

After intravenous injection of heparin (2 mg/kg) for 10 min, $FeCl_3$-injured carotid arteries were prepared as described previously. After 5 min of model preparation, Cy5-uPA (0.5 mg/kg), Cy5-uPA (5 mg/kg), Cy5-uPA/PLTs (0.5 mg/kg) and NO@Cy5-uPA/PLTs (0.5 mg/kg) were injected intravenously. 2 h later, the injured carotid arteries were collected, washed with PBS, fixed in 4% paraformaldehyde, and then treated by freezing microtomy. The frozen sections of injured carotid arteries were stained with DAPI, ICAM-1 and then observed using a confocal microscope (Leica SP8).

2.11. *NO generation of NO@uPA/PLTs*

The Griess reaction was used to measure the NO concentration in the culture supernatant. Briefly, 100 μL of NO@uPA/PLTs dispersed in calcium-free Tyrode's buffer was taken at specified time points. And Griess Reagent I and Griess Reagent II were added to the supernatant obtained by centrifuging the NO@uPA/PLTs. Then the corresponding absorbance was measured at 540 nm using a BioTek Synergy H1 plate reader.

The NO fluorescent probe DAF-FM DA was also used to monitor the Arg-induced NO generation in NO@uPA/PLTs. DAF-FM DA was added into the NO@uPA/PLTs with a final concentration of 5 μmol/L. At specified time points, NO@uPA/PLTs were collected and followed by flow cytometry. The fluorescence intensity of DAF-FM was measured by Flowjo software.

2.12. *NO@uPA/PLTs attenuate HUVEC apoptosis induced by H_2O_2*

HUVEC seeded in 96-well plates were treated with uPA/PLTs or NO@uPA/PLTs in the presence of H_2O_2 (200 μmol/L) for 12 h. After incubation, the medium of each well was replaced with 100 μL of MTT solution. After incubation at 37 °C for 4 h, DMSO (200 μL) was added in each well. And the absorbance at 490 nm was measured using a BioTek Synergy H1 plate reader[35]. The PBS-treated cells were set as the negative control group, and the H_2O_2 (200 μmol/L)-treated cells was set as the positive control group.

DCFH-DA (ROS probe) was also used to measure the ROS level of HUVEC treated with H_2O_2. HUVEC seeded in the cover glass-bottom dishes were treated with uPA/PLTs or NO@uPA/PLTs in the presence of H_2O_2 (200 μmol/L) for 12 h. Then DCFH-DA (5 μmol/L) dissolved in DMSO was added and incubated with cells at 37 °C for 15 min. Then cells were washed with PBS and observed using a confocal microscope (Leica SP8, Germany).

2.13. *The inhibition to platelets activation and aggregation of NO@uPA/PLTs*

Platelets dispersed in calcium-free Tyrode's buffer were incubated with uPA/PLTs, NO@uPA/PLTs, or saline (a total of 1 mL contains platelets: 2×10^8, and 40 μL of uPA/PLTs or NO@uPA/PLTs). After incubation, thrombin (0.2 U/mL, final concentration) or ADP (2.5 μmol/L, final concentration) was added to induce platelets

activation and aggregation. To investigate the inhibition to platelets activation of NO@uPA/PLTs, the platelets were stained with P-selectin antibodies and measured by flow cytometry. To investigate the inhibition to platelets aggregation of NO@uPA/PLTs, the absorbance at 650 nm after incubating 30 min was measured using a BioTek Synergy H1 plate reader. The OD_{650} value of the PBS-treated group was set as 0% platelet aggregation. The percentage of platelet aggregation was calculated with Eq. (1):

$$\text{Platelet aggregation (\%)} = OD_{650\text{Sample}} / OD_{650\text{PBS-treated}} \times 100 \quad (1)$$

To observe the aggregation of platelets more significantly, the fluorescent dye FDA was used to label the platelets. The FDA-labeled platelets suspension was repeated with the same steps as the platelet aggregation experiment. Then the mixture was dropped onto the slide to examine the fluorescence platelets clumps using a confocal microscope (Leica SP8).

2.14. *In vivo therapeutic efficacy studies*

To access pulmonary embolism therapeutic efficacy, the mice were intravenously injected with Cy5-fibrinogen and thrombin sequentially. Five minutes later, uPA, uPA/PLTs, or NO@uPA/PLTs were intravenously injected. After 2 h, the mice were euthanized and the mouse lung tissues were collected. IVIS was used to image mouse lung tissue and Living Image software was used to semi-quantitate the fluorescence intensity of Cy5 through ROI analysis. The lung tissues collected from the mice were also performed by H&E staining for histological examination.

To access inhibitory efficacy of $FeCl_3$-induced carotid arterial thrombosis, the mice were intravenously injected with rhodamine 6G (0.5 mg/kg) to label platelets. After 5 min, uPA, uPA/PLTs, or NO@uPA/PLTs were intravenously injected. After 5 min, the carotid artery was covered with a filter paper (2 mm × 2 mm) saturated by 7.5% $FeCl_3$ solution for 1 min to form a carotid thrombus. At specified time points, the carotid artery was imaged using a stereo zoom microscope. The fluorescent intensity of rhodamine 6G was analyzed using Image J software.

To access therapeutic efficacy of $FeCl_3$-induced carotid arterial thrombus, the mice were intravenously injected with rhodamine 6G (0.5 mg/kg) to label platelets. After 5 min, the carotid artery was covered with a filter paper (2 mm × 2 mm) saturated by 7.5% $FeCl_3$ solution for 1 min to form a carotid thrombus. After 5 min, uPA, uPA/PLTs, or NO@uPA/PLTs were intravenously injected. At specified time points, the carotid artery was imaged using a stereo zoom microscope. The fluorescent intensity of rhodamine 6G was analyzed using Image J software. In addition, the carotid artery was treated with $FeCl_3$ for 1 min once again at 1.5 h after injection of NO@uPA/PLTs. After 30 min, the fluorescent image of carotid artery was collected using a stereo zoom microscope. The fluorescent intensity of rhodamine 6G was quantified using Image J software.

2.15. *Safety evaluation*

The mice were intravenously injected with uPA, uPA/PLTs, NO@uPA/PLTs, and PBS. After 12 h, a small cut 2 cm away from the tail end was made. Then the time required for the tail to stop bleeding was recorded. The blood of mice treated with uPA, uPA/PLTs, NO@uPA/PLTs, and PBS was obtained to access the coagulation indicators, including aPTT, FIB, PT, and TT. And the heart, liver, spleen, lung, kidney, and brain were collected for H&E staining.

2.16. *Statistical analysis*

All data were presented as mean ± standard deviation. Comparison and analysis of multiple groups were conducted by one-way analysis of variance (ANOVA). Statistical significance was considered at $P < 0.05$, and the levels of significance were indicated as $^{*}P < 0.05$, $^{**}P < 0.01$, and $^{***}P < 0.001$.

3. Results

3.1. *Preparation and characterization of NO@uPA/PLTs*

The uPA and arginine (Arg)-coloaded platelet delivery system (NO@uPA/PLTs) was prepared by anchoring uPA in the cellular membrane and intracellularly encapsulating Arg (see Methods). A phospholipid-linked uPA was synthesized by conjugating residual amino groups of uPA with NHS-PEG_{3400}-DSPE (uPA-PEG_{3400}-DSPE) to anchor uPA in the cell membrane. The successful synthesis of uPA-PEG_{3400}-DSPE was validated by polyacrylamide gel electrophoresis. In comparison to uPA, uPA-PEG_{3400}-DSPE demonstrated a significant shift in the gel (as indicated with arrows in Fig. 2A), suggesting an increase in molecular size. The effect of covalent conjugation of PEG_{3400}-DSPE on uPA enzymatic activity was quantified using the chromogenic substrate S-2444. As shown in Supporting Information Fig. S1, uPA-PEG_{3400}-DSPE exhibited enzymatic activity almost identical to that of uPA. To prepare NO@uPA/PLTs, uPA-PEG_{3400}-DSPE and Arg were incubated with platelets freshly isolated from whole blood at different ratios. The loading efficiency and capacity of uPA were 2.57% and 38.5 μg/6 × 10^9 platelets, respectively (Supporting Information Fig. S2A). Arg displayed a loading efficiency of 9.83% and loading capacity of 59.0 μg/6 × 10^9 platelets (Fig. S2B). The successful chimerization of uPA was confirmed by Western blot analysis (Fig. 2B). The lysate of NO@uPA/PLTs possessed a clear band of uPA in the Western blot gel, which was absent when uPA (without PEG-DSPE conjugation) was directly incubated with platelets. The morphology of NO@uPA/PLTs was visualized using both transmission electron microscopy (TEM) and scanning electron microscopy (SEM) (Fig. 2C). NO@uPA/PLTs showed a spherical morphology with a mean diameter of 1.5−2 μm. The stability of anchored uPA in serum was investigated by monitoring the fluorescent change of Cy5-labeled uPA (NO@Cy5-uPA/PLTs, see Methods). After 24 h of incubation with mouse serum, 50% NO@Cy5-uPA/PLTs remained (Supporting Information Fig. S3A and S3B). The fluorescent probe DAF-FM DA was used to measure the NO generation of NO@uPA/PLTs. As shown in Fig. 2D, DAF-FM could be clearly observed in the microscopic image of NO@uPA/PLTs, indicating the successful production of NO. Meanwhile, colocalization of Cy5 and DAF-FM in NO@Cy5-uPA/PLTs (Fig. 2E) further verified the successful preparation of the platelet-based co-delivery system with due functions.

3.2. *NO@uPA/PLTs preserve the bioactivity of platelets*

The rapid elimination of uPA in plasma impairs its thrombolytic effect[7]. The Cy5-labeled platelets (Cy5-PLT, Cy5-uPA/PLTs, Cy5-NO@uPA/PLTs) were injected into ICR mice *via* the tail vein. The

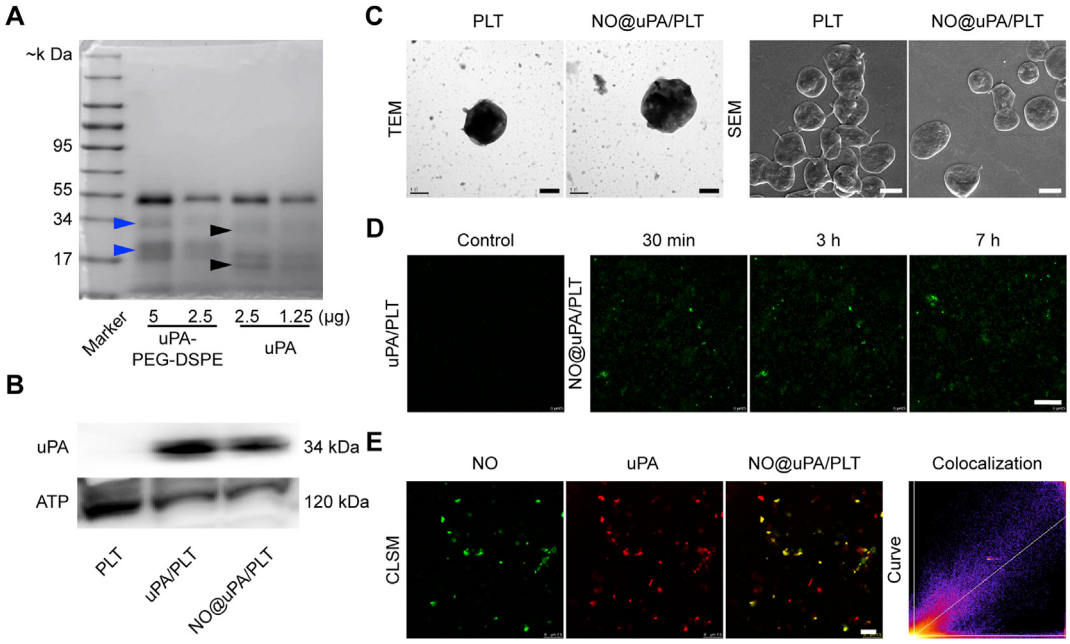

Figure 2 Preparation and characterization of NO@uPA/PLTs. (A) SDS-PAGE gel of PEG-DSPE-conjugated uPA (uPA-PEG-DSPE). (B) Anchored uPA on the platelet membrane characterized using Western blot. Lysates of unmodified platelets (PLTs), uPA-anchored platelets (uPA/PLTs) and uPA/Arg-coloaded platelets (NO@uPA/PLTs) with equal protein amounts were subjected to gel electrophoresis. (C) Representative TEM and SEM images of PLTs and NO@uPA/PLTs. Scale bar indicates 1 μm. (D) Generation of NO in platelets treated with Arg by DAF-FM DA fluorescence staining. Scale bar indicates 50 μm. (E) Representative confocal images of NO@uPA/PLTs. NO was stained with DAF-FM DA (green); uPA was stained with Cy5 (red); scale bar indicates 5 μm.

NO@uPA/PLTs and uPA/PLTs showed a systemic circulation duration similar to that of free platelets (Fig. 3A and B, Supporting Information Fig. S4). Approximately 45% of NO@uPA/PLTs remained in the blood 5 h after injection (Fig. 3C). Compared with free uPA, the blood circulation time of uPA was enhanced after anchored on the platelet membrane. NO@uPA/PLTs activated by thrombin exhibited an amorphous morphology with multiple tentacles and secreted vesicles with a particle size of approximately 200 nm (Fig. 3D and E), similar to the behavior of normal platelets (Supporting Information Fig. S5A and S5B). These results suggested that loading uPA and Arg did not affect the normal physiological functions of the platelets. Meanwhile, platelet microparticles (PMPs) were shed from the activated NO@uPA/PLTs, which were significantly smaller than the resting platelets and helped chimaeric uPA quickly dissolve the thrombus at the thrombus site[36]. NO@uPA/PLTs could aggregate in response to the activation of thrombin or ADP, similar to normal platelets, which was reflected in the change in absorbance of the NO@uPA/PLT suspension at 650 nm (Supporting Information Fig. S6)[37]. Platelets have a natural affinity for inflamed vascular endothelium and fibrinogen[38,39]. Within vascular injury or inflammation, vascular endothelial cells express high levels of adhesion molecules on their surface to enhance their interaction with platelets or leukocytes[40]. TNF-α-stimulated HUVECs were used to mimic activated endothelial cells to evaluate the binding capacity of NO@uPA/PLTs in vascular endothelial cells. The expression of ICAM-1, VCAM-1, and E-selectin in HUVECs after activation by TNF-α was elevated. As shown in Supporting Information Fig. S7, the increase in ICAM-1 expression was the most obvious, showing a level 28 times higher than that in resting cells (Fig. S7D). To test binding with HUVECs, Cy5-NO@uPA/PLTs were incubated with activated and inactivated WGA-Alexa 488-labeled HUVECs. As shown in Fig. 3F and Supporting Information Fig. S8, NO@uPA/PLTs could bind and interact with activated HUVECs. The same experimental results were also observed in the PLT group (Supporting Information Fig. S9). To investigate whether NO@uPA/PLTs could bind to fibrinogen, NO@uPA/PLTs dispersed in calcium-free Tyrode's buffer containing thrombin or not were incubated with Cy5-labeled fibrinogen. After stimulation with thrombin, NO@uPA/PLTs were activated and had a strong affinity for fibrinogen (Fig. 3H). The fluorescence intensity of activated NO@uPA/PLTs associated with fibrinogen was stronger than that of the rest (Supporting Information Fig. S10). The enhanced adhesion of inflammatory endothelial cells and fibrin can give NO@uPA/PLTs a better thrombolytic effect. Dynamic thrombolysis assessment was used to appraise the *in vitro* thrombolysis capacity of NO@uPA/PLTs. The dynamic thrombolysis capacity was assessed by flowing NO@uPA/PLTs over Cy5-labeled fibrin clots in the parallel plate flow chamber system (Fig. 3I). The fibrinolytic effect was evaluated by imaging the red fluorescent clot and observing the fading of red fluorescence under an inverted fluorescence microscope. During the 35-min observation period, there was no obvious fading of red fluorescence in the PBS group, indicating no obvious fibrin degradation. At the end of observation, the residual fibrin clot fluorescence in the uPA group (10 μg/mL) was still 39.5% of that at the original time point. The uPA group (30 μg/mL) effectively lysed clots within 10 min (significant fading of red fluorescence) (Supporting Information Fig. S11). There was no significant difference in the fibrinolytic effect between the NO@uPA/PLT group (10 μg/mL)

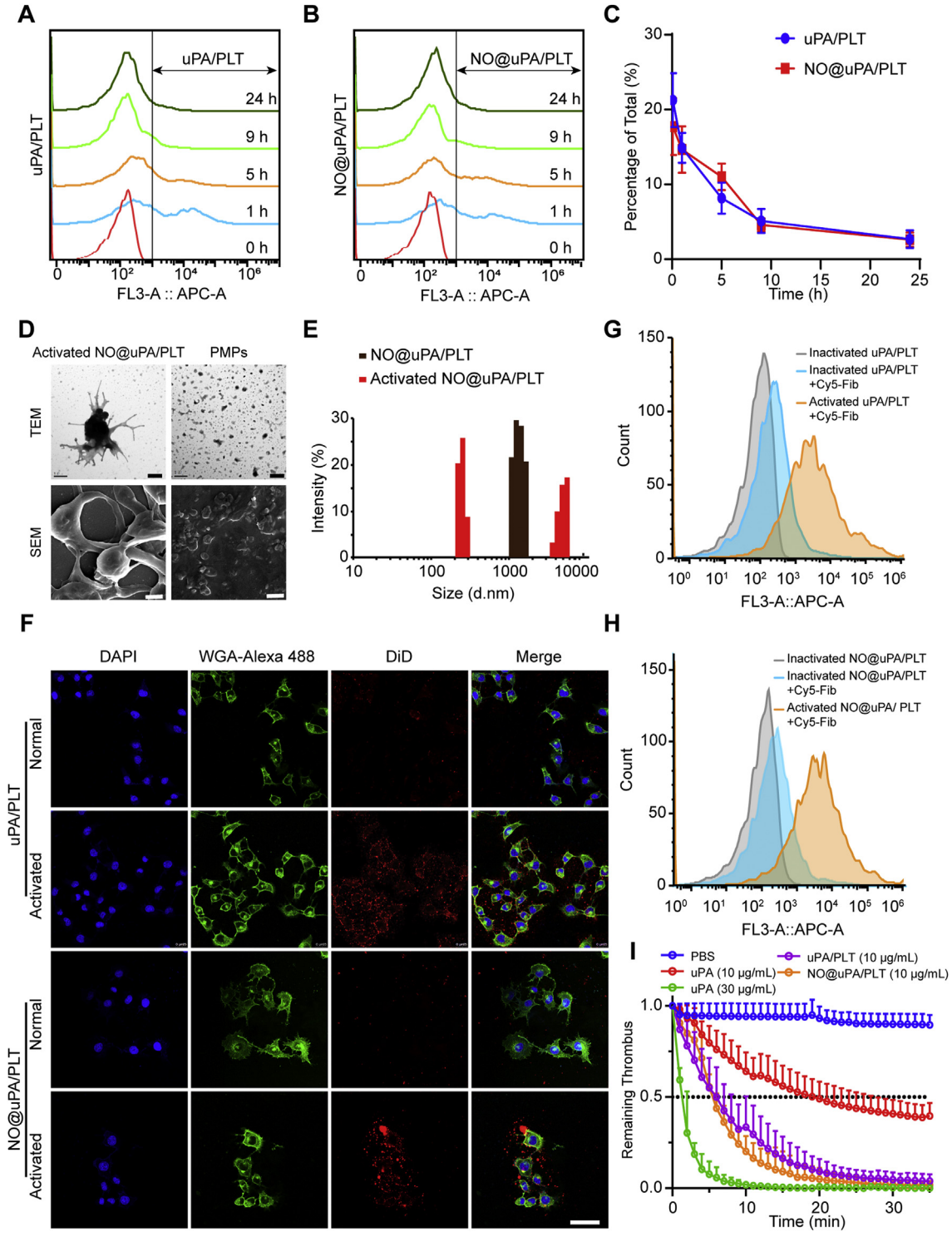

Figure 3 Biological characterization of NO@uPA/PLTs *in vitro* and *in vivo*. Blood circulation retention properties of uPA/PLTs (A) and NO@uPA/PLTs (B). (C) The percentage of uPA/PLTs or NO@uPA/PLTs occupying whole blood platelets at the corresponding time points ($n = 3$). (D) Representative TEM and SEM images of activated NO@uPA/PLTs and released PMPs. Scale bar indicates 1 μm. (E) Size distribution of NO@uPA/PLTs and PMPs. (F) Representative confocal images of uPA/PLTs or NO@uPA/PLTs binding to HUVECs (scale bar indicates 50 μm). Nuclei were stained with DAPI (blue). HUVECs were labeled with WGA-Alexa 488 (green). NO@uPA/PLTs were labeled with Cy5 (red). Scale bar indicates 50 μm. (G) Flow cytometry profiles of inactivated uPA/PLTs and activated uPA/PLTs incubated with Cy5-Fib. (H) Flow cytometry profiles of inactivated NO@uPA/PLTs and activated NO@uPA/PLTs incubated with Cy5-Fib. uPA/PLTs and NO@uPA/PLTs incubated with PBS only were used as negative controls. (I) Thrombotic degradation efficiency of NO@uPA/PLTs within 35 min in the dynamic thrombolysis model. Data are the means ± SD ($n = 3$). *$P < 0.05$. ns, not significant.

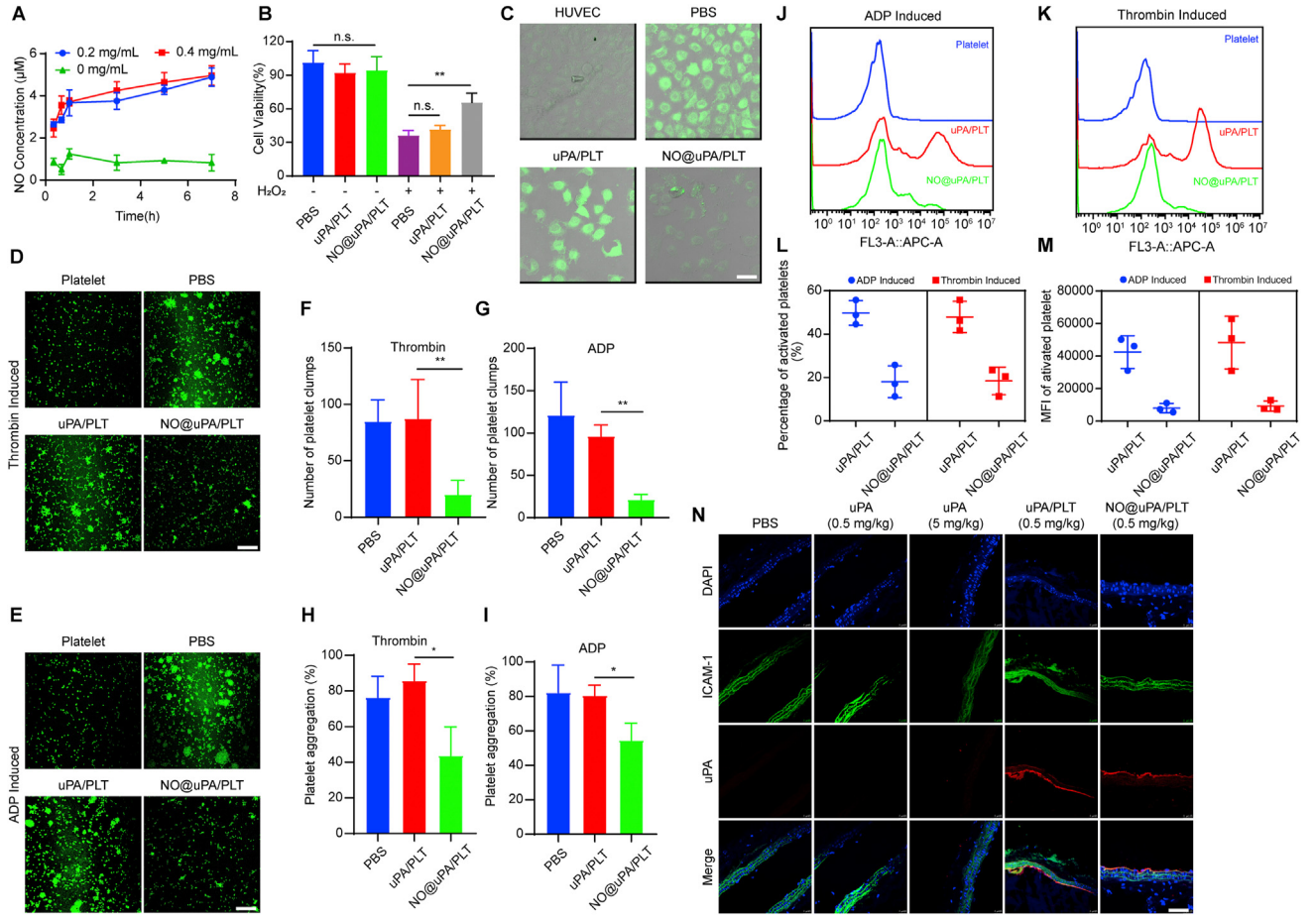

Figure 4 Inhibitory ability of NO@uPA/PLTs against HUVEC apoptosis and platelet activation. (A) Quantification of NO generated by NO@uPA/PLTs incubated with different concentration of Arg using the Griess reaction ($n = 3$). (B) Protective effects of NO generated by NO@uPA/PLTs on H_2O_2-induced HUVECs ($n = 3$). (C) Fluorescent images of HUVECs activated by H_2O_2 after incubation with NO@uPA/PLTs. The scale bar indicates 50 μm. (D, E) Fluorescent images of FDA-labeled platelet aggregation. Platelets were incubated with PBS, uPA/PLTs, or NO@uPA/PLTs, and were activated by thrombin or ADP. The scale bar indicates 50 μm. (F, G) Number of platelet clumps in each field of view in five randomly selected areas under a fluorescence microscope. (H, I) Thrombin-induced (or ADP-induced) aggregation rates of platelets pretreated with PBS, uPA/PLTs, NO@uPA/PLTs ($n = 3$). (J) The expression of P-selectin in ADP-induced platelets pretreated with uPA/PLTs and NO@uPA/PLTs by flow cytometry. (K) Flow cytometry to evaluate the expression of P-selectin in thrombin-induced platelets pretreated with uPA/PLTs and NO@uPA/PLTs. (L) The percentage of activated platelets measured by flow cytometry ($n = 3$). (M) Mean fluorescence intensity of activated platelets measured by flow cytometry ($n = 3$). (N) Representative confocal immunofluorescence images of carotid artery sections after different treatments. Red: uPA; blue: nuclei; green: ICAM-1. Scale bar indicates 50 μm. Data are shown as the mean ± SD ($n = 3$). *$P < 0.05$. n.s., not significant.

and the uPA/PLT group (10 μg/mL), which was significantly stronger than that of the uPA group (10 μg/mL) (Supporting Information Fig. S12).

3.3. *NO@uPA/PLTs attenuate HUVEC apoptosis and inhibit platelet activation*

The NO generation of NO@uPA/PLTs was confirmed by using DAF-FM DA to image NO generation by fluorescence microscopy. As shown in Fig. 2D and Supporting Information Fig. S13, NO@uPA/PLTs showed obvious green fluorescence that was maintained for up to 7 h. This is because loaded Arg can continuously generate NO under the action of NOS in platelets[41]. The level of nitrite in NO@uPA/PLTs was further quantitatively measured using the Griess reagent[42]. After loading Arg, NO@uPA/PLTs continuously generated NO and maintained the NO concentration at 4 μmol/L for up to 7 h, which was significantly increased compared with normal platelets (Fig. 4A). Inflamed endothelial cells can still recruit platelets to adhere to and accumulate in the damaged site of the blood vessel treated with thrombolytics, causing re-embolization[43,44]. HUVECs were treated with H_2O_2 (200 μmol/L) to assess the antioxidant activity of NO@uPA/PLTs (Fig. 4B). After the addition of H_2O_2 (200 μmol/L), a significant reduction in cell viability was observed, and the cell survival rate was reduced to 36.1 ± 4.625%. There was no significant difference in cell

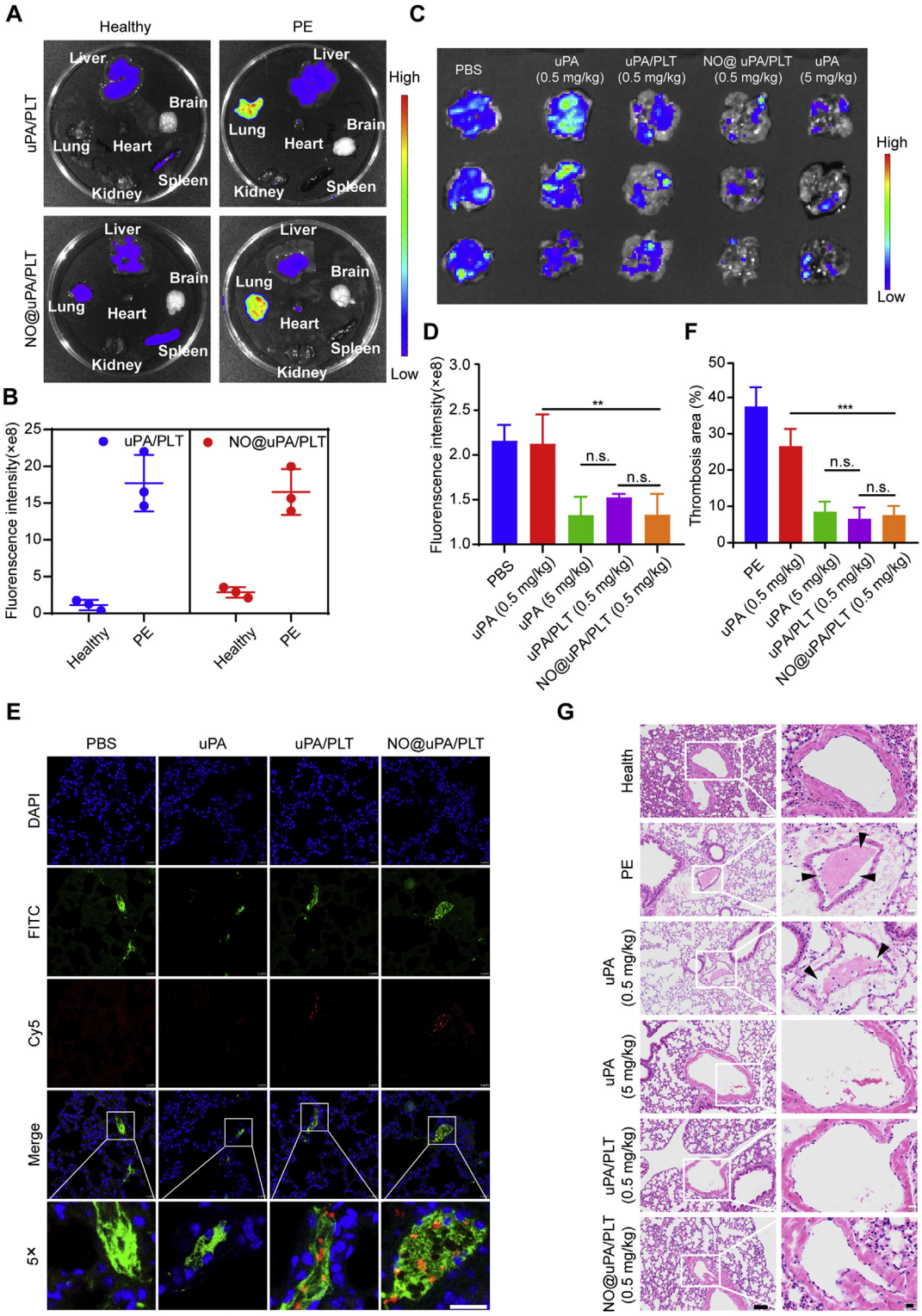

Figure 5 *In vivo* targeting and therapeutic efficacy of NO@uPA/PLTs in the thrombin-induced pulmonary embolism mouse model. (A) Fluorescence images of uPA/PLTs biodistribution and NO@uPA/PLTs biodistribution in the major organs of the PE model and healthy mice. (B) Fluorescence intensity of uPA/PLTs or NO@uPA/PLTs in the lung tissues ($n = 3$). (C) Fluorescent images of the lung tissues harvested from the mice after different treatments. The pulmonary embolism was labeled with Cy5. (D) Fluorescence intensity of Cy5 in lung tissues with different treatments ($n = 3$). (E) *Ex vivo* fluorescent imaging of lung sections from PE mice after treatment with different Cy5-labeled uPA preparations. The scale bar indicates 100 μm. (F) Quantitative analysis of the thrombus area in the lung tissues after different treatments ($n = 3$). (G) Representative H&E staining of lung sections from PE mice after different treatments at 2 h after induction. Scale bar indicates 100 μm. Data are shown as the mean ± SD ($n = 3$). $^*P < 0.05$. n.s., not significant.

viability between the PBS group and the uPA/PLT group, indicating that uPA/PLTs had no protective effects. Interestingly, NO@uPA/PLTs markedly suppressed H_2O_2-induced cytotoxicity, and the cell survival rate increased to 65.62 ± 8.348%. The intracellular level of ROS in H_2O_2-treated HUVECs was measured by confocal microscopy (Fig. 4C). Compared with the uPA/PLT group, NO@uPA/PLTs effectively reduced the level of ROS in HUVECs, exhibiting outstanding HUVEC protective effects. It is important that sufficient NO is provided at the vascular lesion site to inhibit platelet activation and aggregation and subsequent thrombosis[37]. The fluorescence platelet clumps induced by platelet agonists were used to evaluate the platelet aggregation inhibition effect of NO@uPA/PLTs. As shown in Fig. 4D and E, most platelets treated with PBS and uPA/PLTs aggregated into large clumps, but platelets treated with NO@uPA/PLTs were scattered, and the number of clumps was significantly reduced (Fig. 4F and G). Then, the absorbance of the platelet suspension was measured at 650 nm to evaluate platelet aggregation[37]. Neither uPA/PLTs nor NO@uPA/PLTs-induced aggregation of platelets, as evident from Supporting Information Fig. S14. After the addition of platelet agonists, platelets treated with PBS were activated, and aggregation rates reached 76.39 ± 11.93% (thrombin-induced) and 82.21 ± 15.88% (ADP-induced), which were similar to those of platelets treated with uPA/PLTs. However, after incubation with NO@uPA/PLTs, platelet aggregation was significantly inhibited, and aggregation rates reached 43.69 ± 16.26% (thrombin-induced) and 54.43 ± 10.01% (ADP-induced). This finding suggests that NO@uPA/PLTs can reduce the risk of thrombosis reformation by reducing platelet activation and aggregation. NO inhibits platelet activation and aggregation *via* elevation of cGMP levels and reduction of P-selectin expression[45,46]. The antiplatelet effect of NO@uPA/PLTs was investigated by evaluating the P-selectin expression of platelets. After incubation with NO@uPA/PLTs, the platelets stained with P-selectin antibody were measured by flow cytometry. As shown in Fig. 4J and K, P-selectin expression in platelets treated with uPA/PLTs was increased, and the percentage of activated platelets reached 49.77 ± 5.650% (ADP-induced) and 47.93 ± 7.191% (thrombin-induced). In contrast, NO@uPA/PLTs significantly inhibited the expression of P-selectin and reduced the activation rate to 18.07 ± 7.298% (ADP-induced) and 18.43 ± 6.357% (thrombin-induced) (Fig. 4L and M). uPA, which accumulates in vascular injury, can help prevent the recurrence of thrombi. To evaluate the accumulation ability of NO@uPA/PLTs in vascular injury, fluorescence images of frozen sections of injured carotid arteries were collected. The results of the experiment are shown in Fig. 4N. Green fluorescence (anti-ICAM-1) identified the site of carotid vascular injury. The uPA (0.5 mg/kg) and uPA (5 mg/kg) groups exhibited weak red fluorescence signals at the injury site, indicating low concentrations of uPA at the carotid injury site, while the uPA/PLT (0.5 mg/kg) group and NO@uPA/PLT (0.5 mg/kg) group exhibited strong red fluorescence signals, indicating a high concentration of uPA at the site of carotid artery injury, showing that the carried uPA was effectively enriched at the thrombus site to quickly exert the thrombolytic effect and inhibit the reformation of the thrombus. The above experimental results strongly verified the excellent antioxidant capabilities and superior injured carotid artery accumulation of NO@uPA/PLTs, which was beneficial to reverse the high oxidation situation at the injured blood vessel site and inhibit the reformation of thrombi.

3.4. NO@uPA/PLTs enhance the thrombolysis of uPA in a mouse model of thrombin-induced pulmonary embolism

Next, the targeted thrombolytic efficacy of NO@uPA/PLTs was confirmed using a mouse thrombin-induced pulmonary embolism model[47]. The *in vivo* biodistribution of NO@uPA/PLTs in mice with pulmonary embolism was first investigated. Compared with the healthy mice, Cy5-NO@uPA/PLTs accumulated in the lung tissue of pulmonary embolism mice, as proven by the higher Cy5 fluorescence intensity in the lung tissue (Fig. 5A). The results of ROI analysis showed that the fluorescence intensity of NO@uPA/PLTs in the lungs of pulmonary embolism mice was 5.4-fold that of normal mice (Fig. 5B). Owing to the natural tendency of platelets to thrombus, NO@uPA/PLTs showed a better accumulation in pulmonary thrombus. Then, Cy5-labeled fibrinogen was used to evaluate the thrombolytic effect of NO@uPA/PLTs in the pulmonary embolism *in vivo* (see Methods). Two hours after intravenous injection of uPA, uPA/PLTs, or NO@uPA/PLTs, the lung tissues of the mice were imaged by IVIS, and the fluorescence intensity of Cy5-labeled fibrinogen was quantified through ROI analysis. The uPA group (0.5 mg/kg) showed limited thrombolytic effects, as proven by the higher Cy5 fluorescence intensity in the lung. The uPA/PLT group (0.5 mg/kg) and the NO@uPA/PLT group (0.5 mg/kg) both exhibited excellent thrombolytic effects on pulmonary embolism (Fig. 5C and D). Their Cy5 fluorescence intensity in the lung was similar to that of the uPA group (5 mg/kg) due to the ability to specifically target pulmonary embolism. To further confirm whether NO@uPA/PLTs specifically targeted pulmonary embolism, lung sections of embolized mice were observed using a confocal microscope. As displayed in Fig. 5E, a high Cy5-NO@uPA/PLT signal existed at the FITC-labeled pulmonary embolism site in the NO@uPA/PLT group, in contrast to the lower Cy5-labeled uPA signal observed in the uPA group. Haematoxylin and Eosin (H&E) staining was also used to evaluate the thrombotic area of lung tissues. A large-scale embolism of pulmonary blood vessels was observed in the lungs of the PBS group (Fig. 5F). When treated with a high dose of uPA (5 mg/kg), the area of vascular embolism was obviously reduced. Only a few pulmonary blood vessels with embolization were observed in the lungs of the uPA/PLT group (0.5 mg/kg) and the NO@uPA/PLT group (0.5 mg/kg) (Fig. 5G). The results indicated that the chimerization of uPA on platelets promoted the pulmonary accumulation of uPA and the ability to specifically target the embolic site of blood vessels. The above findings indicated that the thrombolytic capacity of uPA was enhanced after chimerizing uPA to platelets.

3.5. NO@uPA/PLTs prevent thrombotic recurrence in the mouse model of $FeCl_3$-induced carotid arterial thrombosis

Next, the $FeCl_3$-induced carotid arterial thrombosis mouse model was established to assess the thrombolytic effect of NO@uPA/PLTs. Rhodamine 6G was injected into mice through the right jugular vein to label platelets, and the thrombus size, reflected by the fluorescence intensity of rhodamine 6G, was monitored in real time to evaluate the inhibitory effect of different uPA preparations on thrombosis (Fig. 6A). The fluorescence intensity of rhodamine 6G remarkably increased in the carotid artery of the PBS-treated mice, indicating $FeCl_3$-induced carotid arterial thrombosis formation. Treatment with free uPA (0.5 mg/kg) had a slight inhibitory effect on thrombosis, as evidenced by a fluorescence intensity similar to that of the PBS group. By comparison, uPA/

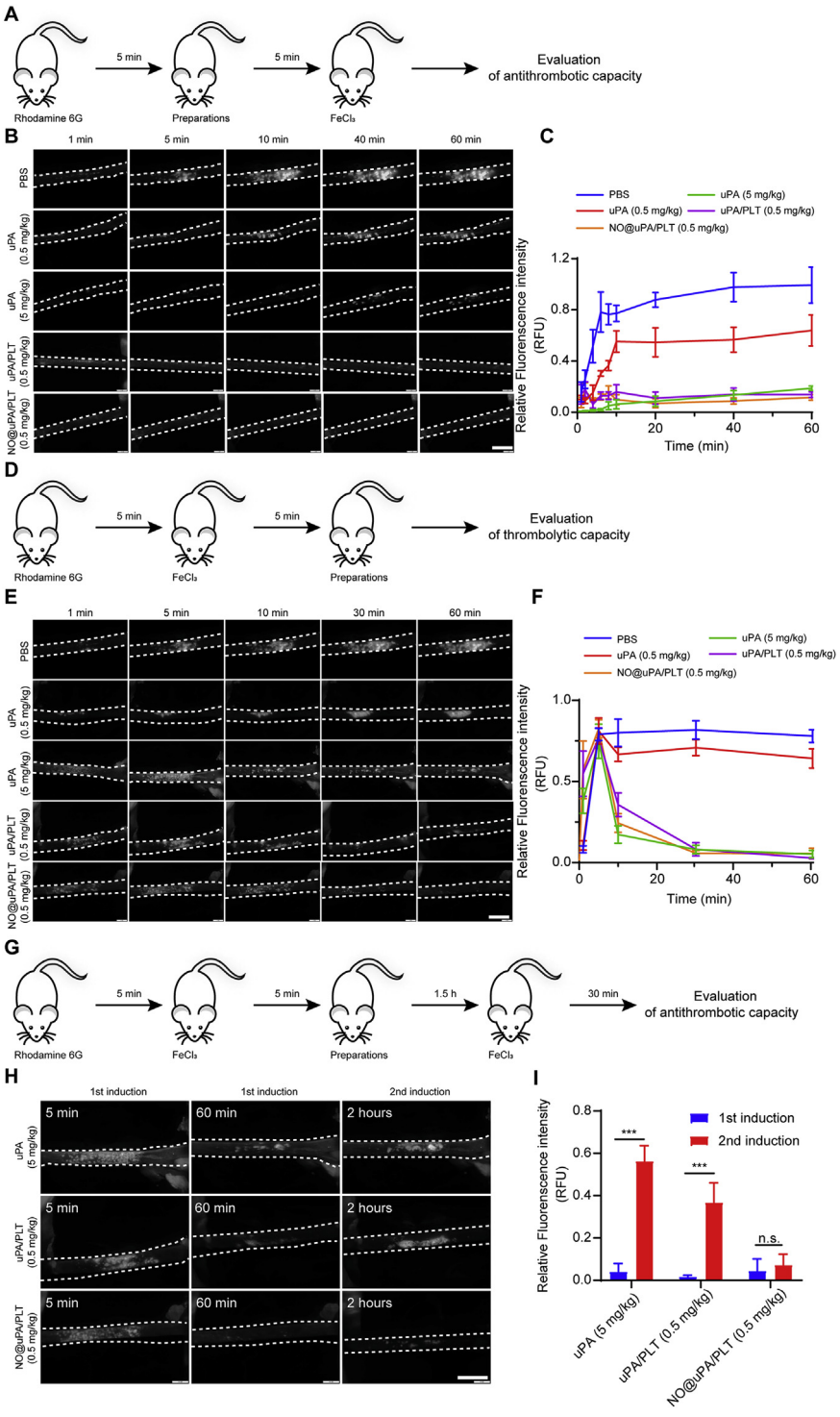

Figure 6 *In vivo* therapeutic efficacy and re-embolism prevention of NO@uPA/PLTs in $FeCl_3$-induced carotid arterial thrombosis models. (A) Schematic illustration of the experimental schedules for the $FeCl_3$-induced carotid arterial thrombosis model. The uPA preparations were injected before thrombosis. (B) Representative fluorescent images of the carotid arteries of the mice after treatment with different uPA preparations at the corresponding time points. (C) Quantification of the rhodamine 6G fluorescence intensity in panel B ($n = 3$). (D) Schematic illustration of the experimental schedules for the $FeCl_3$-induced carotid arterial thrombosis models. The uPA preparations were injected 5 min after thrombosis. (E) Representative fluorescent images of the carotid arteries after treatment with different uPA preparations at the corresponding time points. (F) Quantification of the rhodamine 6G fluorescence intensity in panel E ($n = 3$). (G) Schematic illustration of the experimental schedules for the sequential $FeCl_3$-induced carotid arterial thrombosis models. (H) Representative fluorescent images of the carotid arteries of the mice after treatment with different uPA preparations at the corresponding time points. (I) Quantification of the rhodamine 6G fluorescence intensity in panel H ($n = 3$). Scale bar indicates 400 μm. Data are shown as the mean ± SD ($n = 3$). *$P < 0.05$. n.s., not significant.

PLTs and NO@uPA/PLTs effectively inhibited thrombosis and maintained low fluorescence intensity of rhodamine 6G within 60 min (Fig. 6B and C). uPA/PLTs and NO@uPA/PLTs remarkably suppressed thrombus formation owing to their ability to adhere to the vascular lesion site to provide sufficient uPA. Next, the thrombolytic effect of NO@uPA/PLTs on carotid artery thrombus was evaluated (Fig. 6D). High-dose intravenous infusion of uPA (5 mg/kg) effectively dissolved the existing thrombus, and no increase in intravascular fluorescence intensity was seen at 60 min. As expected, owing to superior thrombus targeting properties and longer circulation duration of platelets, uPA/PLTs and NO@uPA/PLTs can quickly dissolve newly formed thrombi at a dose of 0.5 mg/kg, which was consistent with the thrombolytic effect of the uPA (5 mg/kg) group (Fig. 6E and F). The inhibition of thrombus recurrence of NO@uPA/PLTs was further investigated in the sequential $FeCl_3$-induced thrombosis mouse model with secondary injury (Fig. 6G)[48]. The fluorescence intensity of the mouse carotid artery after two inductions with $FeCl_3$ was monitored by a stereomicroscope (see Methods). In the uPA (5 mg/kg) group and the uPA/PLT group, a markedly higher fluorescence intensity of rhodamine 6G was observed in thrombotic mice after secondary $FeCl_3$ induction than after the first induction, while in the NO@uPA/PLT group, there was no significant difference in the fluorescence intensity of rhodamine 6G between the primary $FeCl_3$ induction and secondary $FeCl_3$ induction. Moreover, the NO@uPA/PLT group had notably lower fluorescence intensity of rhodamine 6G than the uPA/PLT group after the secondary $FeCl_3$ induction (Fig. 6H and I). The above experimental results indicated that NO@uPA/PLTs had an excellent ability to prevent the recurrence of thrombi owing to their ability to inhibit platelet activation and aggregation and protect HUVECs.

3.6. *Safety evaluation*

Tail vein bleeding time was used to evaluate the haemorrhagic risks of uPA/PLTs and NO@uPA/PLTs (Supporting Information Fig. S15A). In contrast to the uPA group (5 mg/kg), which exhibited a longer bleeding time, the uPA/PLTs group and NO@uPA/PLTs group did not show any significant changes in bleeding time. Moreover, the blood and major organs were collected 24 h after administration of different uPA preparations. The serum levels of blood coagulation parameters were quantified, including aPTT (activated partial thromboplastin time), FIB (fibrinogen), PT (prothrombin time), and TT (thrombin time) (Fig. S15B–S15E). There was no significant difference in blood coagulation parameters among the PBS, uPA/PLTs, and NO@uPA/PLTs treatment groups. However, the uPA group (5 mg/kg) exhibited significant changes in these parameters, indicating a high risk of bleeding. For histopathology, the heart, liver, spleen, lung, and kidney were stained by H&E and observed using a microscope (Fig. S15F). There were no obvious pathological changes in the uPA/PLT group or NO@uPA/PLT group. Due to the enhanced thrombolytic effect, NO@uPA/PLTs reduced the dosage of uPA, and showed better coagulation system and organ safety.

4. Discussion

Persistent issues with the direct intravascular administration of thrombolytic agents include their induction of systemic fibrinogenolysis, which causes increased hemorrhagic risk, and their short half-life. While nanotechnology-enabled targeted delivery systems have shown the ability to increase circulatory safety and persistence by encapsulating thrombolytic agents in nanoparticles, the potential immunogenicity of synthetic materials and the complex modification methods of targeted preparations limit their further applications. In this study, inspired by the glycosylphosphatidylinositol anchoring protein on the plasma membrane, uPA was anchored onto the platelet surface by the lipid insertion method. Through lipid insertion technology, uPA was stably retained on the surface of the platelet membrane and was not released into the blood during circulation, thereby preventing the increased risk of bleeding caused by fibrinogenolysis. Due to the intrinsic *in vivo* long circulation characteristics of platelets, the combination of uPA with platelets can extend its half-life *in vivo*. On the other hand, the inherent thrombus affinity of platelets enabled the targeted delivery of uPA to thrombi, which was beneficial for enhancing the thrombolytic effect. The harnessing of platelets as thrombolytic agent carriers provides a simple and effective thrombosis treatment strategy without an urgent need to design complex targeted nanocarriers. Covalent modifications have also been used to bind thrombolytic proteins to biological membranes by functionalizing platelet membrane glycoproteins[11,21,47]. This indiscriminate modification may lead to the loss of function of adhesion molecules and receptors in platelet membranes. In contrast, the lipid insertion method did not change the structure of membrane proteins or induce or inhibit platelet activation, thereby maintaining the normal physiological functions of platelets.

Importantly, co-loading the uPA/Arg platelet delivery system (NO@uPA/PLTs) can reduce the reformation of thrombi compared with that observed for uPA/PLTs. Due to natural platelet tropism, Arg was efficiently delivered to the thrombus site by platelets, and the release of NO in the lesion *in situ* inhibited the activation and aggregation of platelets and protected endothelial cells. NO@uPA/PLTs can effectively prevent re-embolism in the first stage of thrombosis.

In our study, the effectiveness and safety of uPA/PLTs and NO@uPA/PLTs were demonstrated in a mouse thrombosis model. More research is needed on the effectiveness of thrombolysis in large animals, including safety assessments in primates, to achieve clinical applications. Intravenous infusion of platelets has been used to treat the symptoms of thrombocytopenia caused by thrombopoiesis. The source and purity of platelets are the main factors restricting their clinical application. At present, platelets for clinical use are obtained by separating whole blood. The presence of white blood cells in platelet concentrates cause accelerated platelet clearance and the appearance of allogeneic immunity after multiple injections[49,50]. Although it is possible to avoid allogeneic immune reactions by infusing autologous platelets, this may increase the burden on the patient and carry some medical risks. Recently, large-scale production of high-purity platelets *in vitro* has been achieved[51,52]. The engineered platelet-based drug delivery platform has good prospects for clinical application.

In summary, we successfully constructed a uPA/Arg coloaded platelet delivery system, which provided a unique combination to achieve targeted delivery of uPA to thrombi, prolong the duration of uPA circulation and prevent the recurrence of thrombi with limited haemorrhagic risks. This engineered platelet-based drug delivery platform offers an integrated strategy for solving the drawbacks of thrombolytic agents and has great potential to improve the current state of thrombus treatment.

Acknowledgments

We thank the National Center for Protein Science in Shanghai Zhangjiang Laboratory (China) for the use of Leica TCS SP8. This work was supported by the National Natural Science Foundation of China (No.81690263).

Author contributions

Weiyue Lu, Min Liu and Songli Wang designed the research. Songli Wang, Ruifeng Wang, and Nana Meng carried out the experiments and performed data analysis. Linwei Lu, Jun Wang, Jianfen Zhou, Jiasheng Lu, Qianzhu Xu, Cao Xie, Yao Li, and Yang Yu participated part of the experiments. Songli Wang and Ruifeng Wang wrote the manuscript. Weiyue Lu, Min Liu and Changyou Zhan revised the manuscript. All authors have read and approved the final manuscript.

Conflicts of interest

The authors have no conflicts of interest to declare.

Appendix A. Supporting information

Supporting data to this article can be found online at https://doi.org/10.1016/j.apsb.2022.01.004.

References

1. Powers WJ, Rabinstein AA, Ackerson T, Adeoye OM, Bambakidis NC, Becker K, et al. 2018 guidelines for the early management of patients with acute ischemic stroke: a guideline for healthcare professionals from the American heart association/American stroke association. *Stroke* 2018;**49**:e46−110.
2. Kearon C, Akl EA, Ornelas J, Blaivas A, Jimenez D, Bounameaux H, et al. Antithrombotic therapy for VTE disease: CHEST guideline and expert panel report. *Chest* 2016;**149**:315−52.
3. Benjamin EJ, Blaha MJ, Chiuve SE, Cushman M, Das SR, Deo R, et al. Heart disease and stroke statistics-2017 update: a report from the American heart association. *Circulation* 2017;**135**:e146−603.
4. Furie B, Furie BC. Mechanisms of thrombus formation. *N Engl J Med* 2008;**359**:938−49.
5. Derex L, Nighoghossian N. Thrombolysis, stroke-unit admission and early rehabilitation in elderly patients. *Nat Rev Neurol* 2009;**5**:506−11.
6. Molina CA, Montaner J, Arenillas JF, Ribo M, Rubiera M, Alvarez-Sabin J. Differential pattern of tissue plasminogen activator-induced proximal middle cerebral artery recanalization among stroke subtypes. *Stroke* 2004;**35**:486−90.
7. Marder VJ, Novokhatny V. Direct fibrinolytic agents: biochemical attributes, preclinical foundation and clinical potential. *Thromb Haemostasis* 2010;**8**:433−44.
8. Fiorelli M, Bastianello S, Kummer RV, Zoppo GJD, Larrue V, Lesaffre E, et al. Hemorrhagic transformation within 36 hours of a cerebral infarct. *Stroke* 1999;**30**:2280−4.
9. Kaiser Christoph, Pfisterer Matthias. Drug-eluting or bare-metal stents in large coronary arteries. *N Engl J Med* 2011;**364**:1179−80.
10. Ramón L, Ana A, David J, Fernández CC, Paolo P, Wells PS, et al. Dynamics of case-fatalilty rates of recurrent thromboembolism and major bleeding in patients treated for venous thromboembolism. *Thromb Haemostasis* 2013;**110**:834−43.
11. Xu JP, Wang XQ, Yin HY, Cao X, Hu QY, Lv W, et al. Sequentially site-specific delivery of thrombolytics and neuroprotectant for enhanced treatment of ischemic stroke. *ACS Nano* 2019;**13**:8577−88.
12. Li C, Du H, Yang AZ, Jiang SB, Li ZH, Li D, et al. Thrombosis-responsive thrombolytic coating based on thrombin-degradable tissue plasminogen activator (t-PA) nanocapsules. *Adv Funct Mater* 2017;**27**:1703934. 1-11.
13. Voros E, Cho M, Ramirez M, Palange AL, De Rosa E, Key J, et al. TPA immobilization on iron oxide nanocubes and localized magnetic hyperthermia accelerate blood clot lysis. *Adv Funct Mater* 2015;**25**:1709−18.
14. Zhong YX, Zhang Y, Xu J, Zhou J, Liu J, Ye M, et al. Low-intensity focused ultrasound-responsive phase-transitional nanoparticles for thrombolysis without vascular damage: a synergistic non-pharmaceutical strategy. *ACS Nano* 2019;**13**:3387−403.
15. Wang SY, Guo XX, Xiu WJ, Liu Y, Wang LH. Accelerating thrombolysis using a precision and clot-penetrating drug delivery strategy by nanoparticle-shelled microbubbles. *Sci Adv* 2020;**6**:eaaz8204.
16. Cheng R, Huang WJ, Huang LJ, Yang B, Mao LD, Jin KL, et al. Acceleration of tissue plasminogen activator-mediated thrombolysis by magnetically powered nanomotors. *ACS Nano* 2014;**8**:7746−54.
17. Netanel Korin MK, Matthews Benjamin D, Crescente Marilena, Brill Alexander, Mammoto Tadanori, Ghosh Kaustabh, et al. Shear-activated nanotherapeutics for drug targeting to obstructed blood vessels. *Science* 2012;**337**:738−42.
18. Leslie DC, Waterhouse A, Berthet JB, Valentin TM, Watters AL, Jain A, et al. A bioinspired omniphobic surface coating on medical devices prevents thrombosis and biofouling. *Nat Biotechnol* 2014;**32**:1134−40.
19. Pawlowski CL, Li W, Sun M, Ravichandran K, Hickman D, Kos C, et al. Platelet microparticle-inspired clot-responsive nanomedicine for targeted fibrinolysis. *Biomaterials* 2017;**128**:94−108.
20. Pan Y, Ren XT, Wang S, Li X, Luo XL, Yin ZN. Annexin V-conjugated mixed micelles as a potential drug delivery system for targeted thrombolysis. *Biomacromolecules* 2017;**18**:865−76.
21. Xu JC, Zhang YL, Xu JQ, Liu GN, Di CZ, Zhao X, et al. Engineered nanoplatelets for targeted delivery of plasminogen activators to reverse thrombus in multiple mouse thrombosis models. *Adv Mater* 2020;**32**:e1905145.
22. Richardson G, Hicks SL, O′Byrne S, Frost MT, Moore K, Benjamin N, et al. The ingestion of inorganic nitrate increases gastric *S*-nitrosothiol levels and inhibits platelet function in humans. *Nitric Oxide* 2002;**7**:24−9.
23. Jin RC, Voetsch B, Loscalzo J. Endogenous mechanisms of inhibition of platelet function. *Microcirculation* 2005;**12**:247−58.
24. Yenari MA, Kawabori M, Kim JY. Innate inflammatory responses in stroke: mechanisms and potential therapeutic targets. *Curr Med Chem* 2014;**21**:2076−97.
25. Xu LC, Wo Y, Meyerhoff ME, Siedlecki CA. Inhibition of bacterial adhesion and biofilm formation by dual functional textured and nitric oxide releasing surfaces. *Acta Biomater* 2017;**51**:53−65.
26. Qiu H, Qi PK, Liu JX, Yang Y, Tan X, Xiao Y, et al. Biomimetic engineering endothelium-like coating on cardiovascular stent through heparin and nitric oxide-generating compound synergistic modification strategy. *Biomaterials* 2019;**207**:10−22.
27. Stuehr OGD. Nitric oxide synthases: properties and catalytic mechanism. *Annu Rev Physiol* 1995;**57**:707−36.
28. Forstermann U, Sessa WC. Nitric oxide synthases: regulation and function. *Eur Heart J* 2012;**33**:829−37. 37a-37d.
29. Hu CM, Fang RH, Wang KC, Luk BT, Thamphiwatana S, Dehaini D, et al. Nanoparticle biointerfacing by platelet membrane cloaking. *Nature* 2015;**526**:118−21.
30. Wei XL, Ying M, Dehaini D, Su YY, Kroll AV, Zhou JR, et al. Nanoparticle functionalization with platelet membrane enables multifactored biological targeting and detection of atherosclerosis. *ACS Nano* 2018;**12**:109−16.
31. Wang SL, Wang RF, Meng NN, Guo HY, Wu SY, Wang XY, et al. Platelet membrane-functionalized nanoparticles with improved targeting ability and lower hemorrhagic risk for thrombolysis therapy. *J Contr Release* 2020;**328**:78−86.

32. Hao MX, Hou SY, Li WS, Li KM, Zhang C. Combination of metabolic intervention and T cell therapy enhances solid tumor immunotherapy. *Sci Transl Med* 2020;**12**:eaaz6667.
33. Shi GX, Mukthavaram R, Kesari S, Simberg D. Distearoyl anchor-painted erythrocytes with prolonged ligand retention and circulation properties *in vivo*. *Adv Healthc Mater* 2014;**3**:142−8.
34. Fuentes RE, Zaitsev S, Ahn HS, Hayes V, Kowalska MA, Lambert MP, et al. A chimeric platelet-targeted urokinase prodrug selectively blocks new thrombus formation. *J Clin Invest* 2016;**126**:483−94.
35. Ruan HT, Yao SY, Wang SL, Wang RF, Xie C, Guo HY, et al. Stapled RAP12 peptide ligand of LRP1 for micelles-based multifunctional glioma-targeted drug delivery. *Chem Eng J* 2021;**403**:126296.
36. Han X, Chen JW, Chu JC, Liang C, Ma QL, Fan Q, et al. Platelets as platforms for inhibition of tumor recurrence post-physical therapy by delivery of anti-PD-L1 checkpoint antibody. *J Control Release* 2019;**304**:233−41.
37. Li MX, Li J, Chen JP, Liu Y, Cheng X, Yang F, et al. Platelet membrane biomimetic magnetic nanocarriers for targeted delivery and *in situ* generation of nitric oxide in early ischemic stroke. *ACS Nano* 2020;**14**:2024−35.
38. Li JH, Ai YW, Wang LH, Bu PC, Sharkey CC, Wu QH, et al. Targeted drug delivery to circulating tumor cells *via* platelet membrane-functionalized particles. *Biomaterials* 2016;**76**:52−65.
39. Harlan TBBSJ. Adhesion of activated platelets to endothelial cells: evidence for a GPIIbIIIa-dependent bridging mechanism and novel roles for endothelial intercellular adhesion molecule 1 (ICAM-1), $\alpha v\beta 3$ integrin, and GPIbα. *J Exp Med* 1998;**187**:329−39.
40. Pircher J, Engelmann B, Massberg S, Schulz C. Platelet-neutrophil crosstalk in atherothrombosis. *Thromb Haemostasis* 2019;**119**:1274−82.
41. Gawrys J, Gajecki D, Szahidewicz-Krupska E, Doroszko A. Intraplatelet L-arginine-nitric oxide metabolic pathway: from discovery to clinical implications in prevention and treatment of cardiovascular disorders. *Oxid Med Cell Longev* 2020;**2020**:1015908.
42. Miranda KM, Espey MG, Wink DA. A rapid, simple spectrophotometric method for simultaneous detection of nitrate and nitrite. *Nitric Oxide* 2001;**5**:62−71.
43. Gawaz M, Langer H, May AE. Platelets in inflammation and atherogenesis. *J Clin Invest* 2005;**115**:3378−84.
44. Jackson ZKS. The role of platelets in atherothrombosis. *Hematol Am Soc Hematol Educ Program* 2011;**2011**:51−61.
45. Marietta M, Facchinetti F, Neri I, Piccinini F, Torelli G. L-Arginine infusion decreases platelet aggregation through an intraplatelet nitric oxide release. *Nitric Oxide* 1997;**88**:229−35.
46. Libersan D, Rousseau G, Merhi YJTH. Differential regulation of P-selectin expression by protein kinase A and protein kinase G in thrombin-stimulated human platelets. *Thromb Haemostasis* 2003;**89**:310−7.
47. Hu QY, Qian CG, Sun WJ, Wang JQ, Chen ZW, Bomba HN, et al. Engineered nanoplatelets for enhanced treatment of multiple myeloma and thrombus. *Adv Mater* 2016;**28**:9573−80.
48. Xu X, Huang XC, Zhang Y, Shen SY, Mo R. Self-regulated hirudin delivery for anticoagulant therapy. *Sci Adv* 2020;**6**:eabc0382.
49. Sandler Gerald S. Alloimmune refractoriness to platelet transfusions. *Curr Opin Hematol* 1997;**4**:470−3.
50. Claas FHJ, Smeenk RJT, Schmidt R, Steenbrugge GJV, Eernisse JG. Alloimmunization against the MHC antigens after platelet transfusions is due to contaminating leukocytes in the platelet suspension. *Exp Hematol* 1981;**9**:84−9.
51. Smith BW, Rozelle SS, Leung A, Ubellacker J, Parks A, Nah SK, et al. The aryl hydrocarbon receptor directs hematopoietic progenitor cell expansion and differentiation. *Blood* 2013;**122**:376−85.
52. Yukitaka I, Sou N, Naoshi S, Tomohiro S, Yoshikazu K, Mikiko O, et al. Turbulence activates platelet biogenesis to enable clinical scale *ex vivo* production. *Cell* 2018;**174**: S0092867418307360.